

AquaDust: Nanogel reporter of local water potential in-planta

Piyush Jain^{a,1}, Weizhen Liu^{b,f,1}, Jeff Melkonian^c, Duke Pauli^{b,g}, Susan Jean Riha^d, Michael A. Gore^b, and Abraham D. Stroock^{e,2}

^aSibley School of Mechanical and Aerospace Engineering, Cornell University, Ithaca, NY 14853, USA; ^bPlant Breeding and Genetics Section, School of Integrative Plant Science, Cornell University, Ithaca, NY 14853, USA; ^cSoil and Crop Sciences Section, School of Integrative Plant Science, Cornell University, Ithaca, NY 14853, USA;

^dDepartment of Earth and Atmospheric Sciences, Cornell University, Ithaca, NY 14853, USA; ^eSmith School of Chemical and Biomolecular Engineering, Cornell University, Ithaca, NY 14853, USA; ^fCurrent address: School of Computer Science and Technology, Wuhan University of Technology, Wuhan, Hubei 430070, China; ^gCurrent address: School of Plant Sciences, University of Arizona, Tucson, AZ 85721, USA

Leaf water potential is a critical indicator of plant water status, integrating soil moisture status, plant physiology, and environmental conditions. There are few tools for measuring plant water status (water potential) in-situ, presenting a critical barrier for the development of appropriate phenotyping (measurement) methods for crop development and modeling efforts aimed at understanding water transport in plants. Here, we present the development of an in-situ, minimally-disruptive hydrogel nanosensor (AquaDust) for measuring leaf water potential. The gel matrix responds to changes in water potential in its local environment by swelling; the distance between covalently linked dyes change with the reconfiguration of the polymer, leading to changes in the emission spectrum via Fluorescence Resonance Energy Transfer (FRET). Upon infiltration into leaves, the nanoparticles localize within the apoplastic space in the mesophyll; they do not enter the cytoplasm or the xylem. We characterize the physical basis for AquaDust response and demonstrate robust function of AquaDust in intact maize (*Zea mays* L.) leaves as a sensor for water potential. We use AquaDust to perform minimally disruptive field measurements of leaf water potential in response to environmental conditions and measurement of spatial variation of water potential within actively transpiring, intact leaves. AquaDust offers potential opportunities for high-throughput field measurements and spatially resolved studies of water relations within plant tissues.

Responsive hydrogel | Nanobiosensors | Water potential | Plant-water relations

1. Introduction

Plant life depends on water availability. In managing this demand, irrigated agriculture accounts for 70% of all human water use (1); in natural ecologies, a tree can extract 100's liters of water per day from the soil (2). Physiologically, the process of evapotranspiration (ET) dominates this demand for water (Fig. 1A): solar thermal radiation and the unsaturated relative humidity in the atmosphere drive evaporation from the wet internal surfaces of leaves; this water loss pulls water up through the plant's vascular tissue (xylem) and out of the soil. This flow occurs along a gradient in the chemical potential of water, or water potential, ψ [MPa] (3). Studies of water relations and stress physiology over the past decades have found that values of ψ along the path of ET (the soil-plant-atmosphere continuum - SPAC) correlate with growth, crop yield and quality, susceptibility to disease, and the balance between water loss due to ET and the uptake of carbon dioxide

(water-use efficiency) (4–6).

Due to the recognized importance of water potential in controlling plant function, plant scientists have spent considerable effort devising accurate and reliable methods for measuring the water potential of soil, stem, and leaf (7). Of these, in-plant water potential and particularly leaf water potential (ψ^{leaf}) represent valuable indicators of plant water status because they integrate both environmental conditions (e.g., soil water availability and evaporative demand) and plant physiological processes (e.g., root water uptake, xylem transport, and stomatal regulation) (8, 9). To date, techniques to measure ψ^{leaf} remain slow, destructive, or indirect. The current tools (e.g., Scholander pressure chamber, psychrometer, pressure probe) involve disruption of the tissue, the micro-environment, or both (10–12). For example, the widely-used pressure chamber requires excision of leaves or stems for ψ^{leaf} .

Significance Statement

Gaps in our ability to document local water relations in leaves compromise our ability to build complete models of leaf and plant function, and our understanding of ecophysiological phenomena such as response and adaptation to drought. Macroscopically, leaf water potential has been shown to impact vegetative growth, quality and yield of grain and fruit, susceptibility to disease, and, in extreme drought, plant mortality, making it a promising candidate trait to improve water-use efficiency in plants. In this paper, we present a nanoscale sensor (AquaDust) that provides non-invasive measurements of water potential in leaves of intact plants at high spatial and temporal resolution. This creates opportunities for understanding of the mechanisms coupling variations in water potential to biological and physical processes.

P.J., W.L., J.M., S.J.R., M.A.G. and A.D.S. designed research; P.J. and W.L. performed research; P.J., W.L., J.M., S.J.R., M.A.G. and A.D.S. analyzed data; and P.J., W.L., J.M., S.J.R., M.A.G. and A.D.S. wrote the paper.

The authors declare no conflict of interest.

¹P.J. and W.L. contributed equally to this work.

²To whom correspondence should be addressed. E-mail: abe.stroock@cornell.edu

measurements. Other techniques, such as stem and leaf psychrometry, require intimate contact with the tissue, and accurate and repeatable measurements are difficult to obtain (10, 13). These limitations have hindered the study of gradients of water potential along the soil-plant-atmosphere continuum and the development of high-throughput strategies to phenotype based on tissue water potential (14). Additionally, current methods for measuring ψ^{leaf} provide poorly defined averages over tissues in the leaf. This characteristic makes the dissection of water relations on sub-leaf scales challenging, such that important questions remain, for example, about the partitioning of hydraulic resistances within leaves between the xylem and mesophyll (15–17).

These outstanding challenges in the measurement of in-plant water status motivated us to develop the measurement strategy presented here, AquaDust, with the following characteristics: (1) *Non-invasive*: compatible with simple, rapid, non-invasive measurements on intact leaves. Fig. 1B presents our approach in which AquaDust reporters infiltrated into the mesophyll of the leaf provide an externally addressable, optical signal that correlates with the local water potential. (2) *Localized*: allowing for access to the values of water potential at a well-defined location along the path of evapotranspiration in the leaf tissue. Fig. 1C shows a schematic representation of AquaDust particles localized in the apoplastic volume within the mesophyll, at the end of the hydraulic path for liquid water within the plant. (3) *Sensitive and specific*: capable of resolving water potentials close to saturation, across the physiologically relevant range ($\sim -3 < \psi < 0$ MPa) and with minimal sensitivity to other physical (e.g., temperature) and chemical (e.g., pH) variables. Fig. 1D presents a schematic representation of a AquaDust particle formed of hydrogel, a highly tunable material that undergoes a structural response to changes in local water potential (swollen when wet; collapsed when dry). We couple the swelling behavior of the particle to an optical signal via the incorporation of fluorescence dyes (green and yellow circles in Fig. 1D) that undergo variable Forster Resonance Energy Transfer (FRET) as a function of separation. Fig. 1E presents typical AquaDust spectra at high (wet - green curve) and low (dry - yellow

curve) water potentials. A change in water potential leads to a change in the relative intensity of the two peaks in the AquaDust spectrum, such that the relative FRET efficiency, $\zeta = f(I_D, I_A)$, can serve as a measure of water potential. (4) *Inert*: non-disruptive of the physiological properties of the leaf (e.g., photosynthetic capacity, transpiration rate etc.).

In this paper, we present the development, characterization, and application of AquaDust. We show that AquaDust provides a robust, reproducible response of its fluorescence spectra *in situ* to changes in leaf water potential across the usual physiological range. We use AquaDust to measure the diurnal dynamics of ψ^{leaf} under field conditions, with repeated measurements on individual, intact leaves. We further apply our approach to quantify the spatial gradients of water potential along individual leaves undergoing active transpiration and at varying levels of soil-induced drought stress. We conclude that AquaDust offers a powerful new basis for tracking, spatially and temporally, in-plant water potential to study the mechanisms by which it couples to both biological and physical processes to define plant function.

2. Results and Discussion

A. AquaDust design and synthesis. We provide a detailed explanation of the design and synthesis of AquaDust in the S.I. (Sec. S1-S4). Briefly, in the selection of a specific hydrogel matrix, we used literature, theory, and experimentation to guide our design: to minimize dependence on pH, ionic strength, and temperature, we selected poly(acrylamide), a neutral polymer with weakly temperature-dependent swelling (18, 19); to match the range of the swelling transition to the physiological range of water potential ($0 > \psi > -3$ [MPa]), we followed Flory-Rehner theory to tune the polymer fraction (see SI, Sec. S2 A, (20–25)) with the estimate of the chemical affinity of the polymer for water (i.e., the Flory-Chi parameter, χ) as obtained from the swelling behavior of macroscopic gels (see SI, Sec. S3, Table S1). In the selection of specific dyes for the FRET response, we chose fluorophores for which the peaks of excitation and emission fall between the peaks of absorption

of chlorophyll (Fig. 1E), to minimize reabsorption of fluorescence emission of AquaDust; as well as fluorophores such that their emission peaks do not coincide with the peak corresponding to the autofluorescence from leaf so as to minimize the relative contribution from leaf autofluorescence (> 650 nm) while collecting AquaDust fluorescence (Fig. 1E). We used Flory-Rehner theory and dipole-plane FRET model to find iteratively an optimal value of combination of monomer and cross-linker concentration, with fixed dye concentration, to maximize ζ in the range of $0 > \psi > -3$ [MPa] (see SI - Sec. S2 A-C, Fig. S1). Importantly for the robustness of AquaDust as spectral reporters of local water potential, we find that a combined theory based on Flory-Rehner swelling and dipole-plane FRET interactions allows us to describe the function, $\zeta(\psi)$ with a single adjustable parameter (the effective inter-dye separation in the swollen state) (see SI - Sec. S1 D, S2, S3, and Fig. S2, S3).

In defining the size of AquaDust particles, the need to deliver them through the stomata and to minimize obstruction of internal cavities within the mesophyll set a micrometer-scale upper bound; the need to accommodate FRET pairs with separations ranging from 4 to 10 nm and avoid passage through the pores of cell walls set a 10 nm-scale lower bound (it is reported that the nanoparticles sized less than 10 nm can translocate through the cell wall pores (26)). To achieve size control, we synthesized hydrogel nanoparticles using inverse microemulsion polymerization technique with Acrylamide (AAm) as the monomer and N-aminopropyl methacrylamide (APMA) as a primary amine-bearing comonomer for reaction with donor and acceptor fluorophores conjugated via N-hydroxysuccinimidyl ester (27–30)(see SI for details on AquaDust synthesis, Sec. S4 A-B, Fig. S4). We chose an appropriate water-to-oil ratio and surfactant concentration to regulate the size of the aqueous core of the reverse micellar droplets (31). After synthesis, the size of these nanoparticles was 42 nm (number-averaged mean) with a standard deviation of 13 nm, as measured using the dynamic light scattering technique (see SI, Sec. S4 C, Fig. S5).

B. AquaDust characterization and *in situ* calibration. We used maize (*Zea mays* L.) as the model species for infiltrating and calibrating AquaDust. Maize leaves have an alternating array of regularly-spaced stomata and vascular bundles with inter-connected air spaces beneath the stomata in the axial (vein) direction, which allows for infiltration in axial direction (32). We infiltrated AquaDust in the leaves by injecting the suspension with pressure through the abaxial surface of the intact leaf (see SI - Fig. S6). We used AquaDust concentration of 6.6×10^8 particles ml⁻¹, with deionized water as solvent medium; the choice of concentration was such that AquaDust fluorescent intensity was 10 fold higher than the leaf autofluorescence to improve signal to background ratio, and no salts were used in the suspension in order to minimize particle aggregation prior to infiltration (see SI - Sec. S4 C for details).

Immediately, after the infiltration, the zone into which the suspension permeated appeared dark (Fig. 2A); in maize, this zone typically extended ~ 6 mm laterally and ~ 4 cm axially from the point of injection. We allowed the infiltrated suspension to come to equilibrium in the leaf under standard growing conditions for 24 hours before measurement of water potential; at this time, the appearance of the infiltrated zone returned to that of the surrounding, non-infiltrated tissue. At the site of infiltration, we typically observed some mechanical disturbance of the cuticle. We avoided interrogating AquaDust at this spot as discussed below.

Fig. 2B shows the autofluorescence from the symplasm of the bundle sheath cells and mesophyll cells (false-colored as blue), as acquired by confocal fluorescence microscopy (see SI - Sec. S4 D for details). In the top-view micrograph of the leaf without AquaDust, the autofluorescence false-colored as blue denotes the symplasm of mesophyll and bundle sheath cells (33) (See SI - Sec. S4 D for details on sample preparation, Fig. S6 for cross-section view). In the top-view micrograph of an intact leaf infiltrated with AquaDust, and upon letting the buffer evaporate, the excitation of AquaDust resulted in fluorescence false-colored as yellow (Fig. 2C). We see that AquaDust was co-located with the cell walls, predominantly in areas exposed to vapor pockets within the mesophyll as seen in the micrograph shown in Fig. 2C.

This distribution suggests that the AquaDust particles mostly coat rather than penetrate the cell wall. We note that we do see some evidence of penetration into non-exposed apoplastic spaces (e.g., between adjacent cells), despite the expectation that the particles >10 nm in diameter should be excluded from passage through cell wall (26). Some permeation of the nanoporous cell wall may be allowed by the soft nature of the gel particles. Fig. 2C clearly shows that the AquaDust was excluded from the cytosol of all cells (mesophyll, epidermal and bundle sheath cells), and from the vascular bundles. Images of full cross-section show this localization pattern continues through the full section of the leaf (see SI - Fig. S6 for the cross-section view of leaf with and without AquaDust). Importantly, the localization of AquaDust with the apoplast places it at the end of the transpiration path, providing an unprecedented opportunity to probe the thermodynamic state of water at the sites of gas exchange with the atmosphere.

To assess the effect of AquaDust infiltration on the leaf physiological function, we compared the CO₂ and water vapor exchange rates between areas of maize leaf with and without infiltration of AquaDust. We observed no significant impact of AquaDust on leaf physiological parameters (see SI, Sec. S4 E, Table S2). In order to deploy AquaDust in living plant tissues as water potential sensor, it is crucial to minimize AquaDust response to other physical and chemical variables such as temperature and pH. We found negligible changes in AquaDust emission spectra over a relatively broad temperature range ($\sim 11 - 21^\circ\text{C}$) (see SI - Sec. S4 F, Fig. S7) (34). This observation is consistent with the reported studies on negligible change in swelling of acrylamide gel in response to temperature (18, 19). Also, the normalized AquaDust emission spectra were slightly sensitive (within the uncertainty range of water potential measured using AquaDust as described in next section) over a pH range of 5-11 because of the use of non-ionic, unhydrolyzed polyacrylamide gels used in the synthesis of AquaDust (see SI - Sec. S4 G, Fig. S8) (35–37).

C. In-planta measurements and calibration. In order to perform non-invasive interrogations of the state of AquaDust within the leaf tissue, we developed the platform illustrated in Fig. 3A: we used an excitation source (mercury halide light

source), appropriate excitation and collection filters, optical fiber probes, a leaf clamp designed to block the ambient light and to position the reflection probe, and a spectrometer to collect the fluorescence emission spectra (see details in SI, Sec. S4 H, Fig. S9). A typical measurement takes <30 seconds. Fig. 3B shows the emission spectra from AquaDust on an intact maize (*Zea mays* L.) leaf as we subjected the potted plants to dry-down in order to progressively reduce the ψ^{leaf} (for details, see SI - Sec. S4 I). We observe qualitative changes in the fluorescence spectrum from the leaf: the relative intensity of the acceptor dye at ~ 580 nm rises with decreasing leaf water potential as measured using pressure chamber ($\psi_{\text{PC}}^{\text{leaf}}$, see SI- Sec. S4 I for details on how pressure chamber measurement was performed). Importantly, this large change in intensity occurs over a range of ψ^{leaf} typically encountered during plant water stress for most agriculturally relevant species, including maize (0 to -1.5 MPa) (38).

The spectra in Fig. 3B allowed us to calibrate the AquaDust response relative to the pressure chamber. From AquaDust emission spectra (Fig. 3B), we extracted the experimental values of relative FRET efficiency, ζ_{exp} , as a function of the ratio of intensity of the acceptor peak (~ 580 nm) to that of the donor peak (~ 520 nm) (see SI, Sec. S3 C). In Fig. 3C, we plot ζ_{exp} from the emission spectra (Fig. 3B) against the $\psi_{\text{PC}}^{\text{leaf}}$ (see SI - Table S3 for the numerical values). The measured values of FRET efficiencies fit a first-principles model (dashed curve) that couples the hydrogel swelling as a function of water potential (Flory-Rehner) and the FRET interaction (dipole-plane interaction (39–41); for details on comparison with other models, see SI - Sec. S2 B,D, Fig. S2). As with the ex-situ calibration (see SI - Fig. S3), this in-situ calibration involved adjusting a single parameter, c (separation of dyes at saturation) to fit the theoretical FRET efficiency to the experimental FRET Efficiency ($\zeta_{\text{th}} = \zeta_{\text{exp}}$) at a single measurement point (here, closest to saturation: $\psi_{\text{PC}}^{\text{leaf}} = -0.08$ MPa) to represent accurately the response across the full range. The requirement of a single calibration measurement limits the time required to initiate use of each new batch of AquaDust as sensor for measuring water potential. This robust, simple behavior was reproducible across the plants we have investigated

(including other species such as Coffee (*Coffea*) and Tomato (*Solanum lycopersicum* L.) leaves) and was stable for at least 5 days in fully illuminated conditions in the greenhouse (see SI - Sec. S4 I for greenhouse conditions).

Averaged over all the readings, the difference between mean value of $\psi_{\text{AQD}}^{\text{leaf}}$, and the mean value of $\psi_{\text{PC}}^{\text{leaf}}$, is 0.018 MPa with a standard deviation of 0.067 MPa. Based on the uncertainty associated with the experimental value of $\psi_{\text{PC}}^{\text{leaf}}$ and multiple measurements from AquaDust, we found that the uncertainty in $\psi_{\text{AQD}}^{\text{leaf}}$ is ± 0.14 MPa based on 95% confidence interval estimate for the model compared with ± 0.05 MPa for the Scholander pressure chamber (see SI for analysis - Sec. S4 J, Fig. S10). This uncertainty is sufficiently small for most studies of water relations given the range of ψ^{leaf} typically encountered during plant water stress is 0 to -1.5 MPa.

As noted before, we observed mechanical damage on cuticle during injection of AquaDust by pressure infiltration (Fig. 2A) ; this could result in AquaDust around the site of injection being exposed to the external vapor environment. We found that the water potential reading from AquaDust was uniform and stable ± 3 mm away from the point of infiltration (see SI - Sec. S4 K, Fig. S11). As a result, measurements from AquaDust were taken > 1 cm away from the site of injection to be considered as a reliable measure of ψ^{leaf} . Since the extent of AquaDust infiltration is on the order of $\gtrsim 4$ cm for a single infiltration in maize (Fig. 2B), the effect of damage due to injection could be reasonably avoided.

D. Documentation of diurnal variation in leaf water potential in intact plants. The relative rates of water loss (evapotranspiration) and water uptake controls the water status of a plant. Variations in evaporative demand, which is a function of net radiation, relative humidity, air temperature and wind speed, and soil water status, as well as physiological responses of the plant, result in fluctuations in ψ^{leaf} . To date, access to the dynamics of in-plant water stress in the field has required destructive sampling of tissues (e.g., one leaf per measurement with pressure chamber) or inference from measurements in the soil and atmosphere. One of the advantages of AquaDust is that it provides non-invasive measurements in intact plant tissues and hence, can be used for repeated measurements of water status on individual

leaves to track dynamics. The response time of the AquaDust to a step change in water potential occurs on the order of seconds (See SI - Sec. S4 L, Fig. S12). The response time of leaves to the changes in environmental conditions is expected to be on the order of 15 minutes (42); hence, AquaDust opens up opportunities to study water stress response of leaves to changing external environmental conditions.

We found general agreement between calibration of AquaDust in growth chamber and the calibration of AquaDust in field conditions (see SI - Sec. S4 M, Fig. S13 for details). Once, calibrated, we documented the changes in $\psi_{\text{AQD}}^{\text{leaf}}$ of maize leaves over a period of 15 hours in a well-irrigated field (minimal effect of soil moisture status). We performed measurements on two adjacent maize plants in an instrumented research plot at Cornell's Musgrave Farm (see SI - Fig. S14 A) in which eddy covariance provided an estimate of rates of evapotranspiration (ET) and solved for canopy conductance (Fig. 4 A,B) using the Penman-Montieth equation (using measured biomet. data, see SI - Sec. S4 N, Fig. S14). With AquaDust infiltration in leaves 4 and 7, we acquired three measurements per leaf once or more per hour throughout the day (except during field irrigation between 07:00 and 10:00). These measurements of the diurnal dynamics of $\psi_{\text{AQD}}^{\text{leaf}}$ agree favorably with the predictions of a potential driven water uptake model (43) (for details, see SI - Sec. S5 N, Fig. S13) which is used to simulate ψ^{leaf} , based on actual evapotranspiration and soil water status, calibrated on this site over several years (Fig. 4B-D, see SI - Sec. S5 N). This demonstrates the potential for AquaDust to track crop water status under variable climate conditions with minimally perturbative, rapid and repeated measures of ψ^{leaf} .[Jeff: What can we say about mid-day values of aquadust leaf water potential measurement that do not match the model?]

E. Water potential gradients along the leaf. AquaDust opens a route to investigate local water potentials to understand and model water potential gradients in plants. As an example, here, we used AquaDust to track changes in ψ along a leaf blade to characterize key resistances to water flow in leaves.

Water moves from the petiole axially through the xylem and laterally from xylem into the surrounding mesophyll, down water potential gradients resulting from the

flux of water out of the surfaces of the leaf. One primary cause of productivity loss during drought is the increase in hydraulic resistance that reduces the water flow to the site of photosynthesis (9, 15, 44). The whole-leaf hydraulic resistance has often been measured by recording the changes in the flux of water in excised leaves with varying degrees of water stress (ψ^{leaf}) (45). Hydraulic decline with decreasing ψ^{leaf} has been primarily attributed to the embolism of xylem vessels (46–49) as assessed by either indirect acoustic (46, 50, 51) or imaging (52–54) techniques. However, these techniques lack quantitative information on the fraction of decline in hydraulic conductance that can be attributed to loss of xylem conductance. Recent experimental studies involving quantitative measurements of leaf xylem conductance (55, 56) and other modeling studies (57, 58) have suggested that the extra-vascular resistance can contribute to > 75% of the total leaf resistance upon dehydration, on average. However, these experimental studies have relied on excised plant material and vein cutting (vacuum chamber method) to partition the relative roles of xylem embolism and changes in outside-xylem properties to explain the whole-leaf hydraulic decline (55, 56). Significant uncertainty remains in the interpretation of these resistances in terms of local physiology due to the average nature of the measurement of ψ^{leaf} and the need to disrupt the tissue to gain hydraulic access to the xylem (59).

Here, we demonstrated the use of AquaDust to monitor in-situ water potential gradients in an intact, mature, transpiring maize leaf during a developing soil moisture stress. Fig. 5A shows, schematically, where we infiltrated AquaDust into maize leaves for measurements of local ψ^{leaf} gradients along the leaf. Fig. 5B shows the $\psi_{\text{AQD}}^{\text{leaf}}$ on node($z = L/6$), mid($z = L/2$), and tip($z = 5L/6$) of the maize leaf. Under the well-watered (WW) conditions, we observed a gradient ranging from 0.11 to 0.22 MPa/m from the node to tip of the leaf with an average transpiration rate of $E = 3.4 \times 10^{-5} \text{ kg}/(\text{m}^2 \cdot \text{s})$ ($\pm 0.7 \times 10^{-5} \text{ kg}/(\text{m}^2 \cdot \text{s})$ (range), as measured using GFS3000, Walz Inc. and averaged over 6 measurements on 3 well-watered and 3 water-limited plants on Day 3, see SI - Sec. S5 A for details). Similar values of transpiration-induced gradients were reported for maize leaves, as measured using

isopiestic psychrometer (gradient of 0.17 MPa/m, $E = 2.9 \times 10^{-5}$ kg/(m².s), (60)), and gradients predicted from the hydraulic architecture model for maize leaves (gradient of ~ 0.1 MPa/m, $E = 2.6 \times 10^{-5}$ kg/(m².s), (61)). However, the use of a cell pressure probe is limited by the range of water potential that can be measured (<-0.7 MPa) (61) as well as the lack of agreement between ψ^{leaf} measured using a xylem pressure probe and a Scholander pressure chamber for ‘transpiring’ leaves (62). We observed that during a developing soil moisture stress, the water potential at the tip of the leaf decreases significantly relative to the mid and the node of the leaf (Fig. 5B). Indeed, the potential drop from node to tip in plant with limited water supply (WL) for more than 1 day was 3-fold larger than that from the node to tip in a well-watered (WW) plant (Fig. 5B), indicating a substantial loss of conductance in the stressed leaves. In analyzing the trends observed in Fig. 5B for WW and WL gradients, we can take advantage of the localization of AquaDust in the mesophyll, outside the xylem at terminal end of the hydraulic pathway (Fig. 2D). This localization allows us to test hydraulic models of the intact leaf with explicit hypothesis about the partitioning of resistance between the xylem and outside xylem components of the pathway. We hypothesize a case where xylem only presents limiting resistance to water flow (see SI - Sec. S5 B, Fig. S15) and find that the complete lack of agreement between the xylem water potential ($\psi_{\text{th}}^{\text{xyl}}$) and $\psi_{\text{AQD}}^{\text{leaf}}$ suggests additional resistances must separate site of AquaDust measurement from xylem.

Fig. 5C presents hydraulic circuit with $\psi_{\text{th}}^{\text{xyl}}$ -dependent xylem resistance (R_{xyl}) and extra-vascular resistances (R_{ox}) separating the xylem from the sites of our measurements. For xylem resistance, we fit logistic function to the vulnerability curve for xylem as reported in literature (61, 63) (see SI - Sec. S5 B). We consider $R_{\text{ox}}(\psi_{\text{th}}^{\text{ox}})$ to be a logistic function of outside-xylem water potential, $\psi_{\text{th}}^{\text{ox}}$. We optimize for the parameters of the logistic function to fit the $\psi_{\text{AQD}}^{\text{leaf}}$ in WW and WL plants. Specifically, we found the minimum mesophyll resistance ($R_{\text{ox}}(\psi = 0)$) and $\psi_{\text{th},50\%}^{\text{ox}}$ (ψ corresponding to 2-fold increase in hydraulic resistance) to minimize the difference between $\psi_{\text{th}}^{\text{xyl}}$ and $\psi_{\text{AQD}}^{\text{leaf}}(\pm \text{range})$ in WW and WL plants. Correspondingly, we

obtained $R_{\text{ox}}(\psi = 0)$ to be ~ 4 times that of $R_{\text{xyl}}(\psi = 0)$ and $\psi_{\text{th},50\%}^{\text{ox}} = -0.6$ MPa. We found that the corresponding prediction of $\psi_{\text{th}}^{\text{ox}}$ could explain $\psi_{\text{AQD}}^{\text{leaf}}(\pm \text{range})$ for all Day 1, Day 2 and Day 3 WL plants (Fig. 5D). Similar values and ψ -dependence for extra-vascular resistance were reported for the mesophyll resistance obtained for different species using vacuum pressure method and modeling studies (55, 56).

We find that the resistance to water flux inferred to explain the gradients in water potential is consistent with the resistances reported in literature using excised plant tissues. The good agreement between $\psi_{\text{AQD}}^{\text{leaf}}$ and $\psi_{\text{th}}^{\text{ox}}$ supports existing assessment of leaf hydraulics (extra-vascular resistance are dominant). The agreement between $\psi_{\text{AQD}}^{\text{leaf}}$ and $\psi_{\text{th}}^{\text{ox}}$ also reinforces the assumption that AquaDust measures outside-xylem water potential. Our observations demonstrate the capability of AquaDust as an in-situ sensor of local ψ and precise localization in mesophyll to help better understand the spatial dynamics of ψ^{leaf} and aid more realistic modeling efforts aimed at understanding local scale water transport in leaves.

3. Conclusion

Our approach of hydrogel based nanosensors, AquaDust, allows for in-situ, non-invasive measurement of water potential in local physiologically-relevant micro-environment. It opens up opportunities for better understanding of physics and biology of water dynamics in plants. As the process of AquaDust infiltration in leaves and fluorescence readout matures, AquaDust could be used for a high-throughput phenotyping strategy that allows for the discovery and quantification of new traits impacting water-use efficiency in crops. AquaDust also allows to identify specific, localized resistances to liquid water flux, and as an indirect indicator of genotypic variation in root architecture (64), it could be part of a larger effort to develop crop genotypes or ‘ideotypes’ for particular drought stress environments with the goal of improving crop adaptation and increasing crop productivity in these environments. AquaDust, given its scale and localization within the mesophyll, also provides opportunities to map gradients of water potential driving water flux from xylem to mesophyll and to atmosphere and identifying the major resistances along the

pathway from petiole to the sites of evaporation. It also opens up possibilities to address key questions that center on providing an independent estimate of the water potential of the evaporative surfaces during transpiration, critical in measurements of exchange of carbon dioxide and water vapor (65, 66). AquaDust can also be useful in non-plant contexts, including, for example, measuring humidity in micro/nano-environments at a cellular level to assess the biological behavior with environmental parameters and in abiotic contexts, such as, to obtain readable output of water potential in food products, soils and synthetic materials.

Materials and Methods

Materials and methods for synthesis, characterization, calibration and usage of AquaDust is described in SI.

ACKNOWLEDGMENTS. The authors would like to acknowledge the technical assistance of Glenn Swan and Nicholas S. Kaczmar; Prof. William Philpot for providing ST2000 spectrometer and optical fiber probes; Prof. Ying Sun, Dr. Christine Yao-Yun Chang and Jiaming Wen for their technical assistance with using GFS3000 gas exchange measurement device and pressure chamber; Prof. Jocelyn K. C. Rose and Dr. Iben Sorensen for their technical support for sample preparation for the confocal imaging; Prof. Warren R. Zipfel and Dr. Rebecca M. Williams for their assistance with u880 confocal microscope imaging; Dr. Olivier Vincent for assistance in using vacuum setup; and Jacob L. Wszolek in Cornell Guterman Lab for maintaining the plants in greenhouse and growth chamber. This work was supported by the Agriculture and Food Research Initiative Competitive Grant no. 2017-67007-25950 from the USDA National Institute of Food and Agriculture and Cooperative Research Program for Agriculture Science and Technology Development (Project No. PJ01321305) Rural Development Administration, Republic of Korea. This work was performed in part at Cornell University Biotechnology Resource Center (NIH S10RR025502 for data collected on the Zeiss LSM 710 Confocal, NIH S10OD018516 for data collected on the upright Zeiss LSM880 confocal microscope (u880)), and in part at the Cornell NanoScale Facility, a member of the National Nanotechnology Infrastructure Network (National Science Foundation, grant no. ECCS-1542081).

1. FAO (2017) *Water for Sustainable Food and Agriculture*. p. 33.
2. Meinzer FC, Bond BJ, Warren JM, Woodruff DR (2005) Does water transport scale universally with tree size? *Functional Ecology* 19(4):558–565.
3. Stroock AD, Pagay VV, Zwieniecki MA, Michele Holbrook N (2013) The Physicochemical Hydrodynamics of Vascular Plants. *Annual Review of Fluid Mechanics* 46(1):615–642.
4. Schulze ED (1986) Carbon Dioxide and Water Vapor Exchange in Response to Drought in the Atmosphere and in the Soil. *Annual Review of Plant Physiology* 37(1):247–274.
5. Shackel K (2011) A plant-based approach to deficit irrigation in trees and vines. *HortScience* 46(2):173–177.
6. McCutchan H, Shackel K (1992) Stem-water Potential as a Sensitive Indicator of Water Stress in Prune Trees (*Prunus domestica* L. cv. French). *Journal of the American Society for Horticultural Science* 117(4):607–611.
7. Turner NC (1981) Techniques and experimental approaches for the measurement of plant water status in *Plant and Soil*. Vol. 58, pp. 339–366.
8. Nobel PS (1999) *Physicochemical and Environmental Plant Physiology*. (Academic Press), 2nd edition.
9. Choat B, et al. (2012) Global convergence in the vulnerability of forests to drought. *Nature* 491(7426):752–755.
10. Wullschleger SD, Dixon MA, Oosterhuis DM (1988) Field measurement of leaf water potential with a temperature-corrected in situ thermocouple psychrometer. *Plant, Cell & Environment* 11(3):199–203.
11. Dixon MA, Tyree MT (1984) A new stem hygrometer, corrected for temperature gradients and calibrated against the pressure bomb. *Plant, Cell & Environment* 7(9):693–697.
12. Scholander PF, Hammel HT, Bradstreet ED, Hemmingsen EA (1965) Sap Pressure in Vascular Plants: Negative hydrostatic pressure can be measured in plants. *Science* 148(3668):339–46.
13. Martinez EM, Cancela JJ, Cuesta TS, Neira XX (2011) Review. Use of psychrometers in field measurements of plant material: accuracy and handling difficulties. *Spanish Journal of Agricultural Research* 9(1):313.
14. Kramer PJ, Boyer JS (1996) *Water Relations of Plants and Soils*. Vol. 161, pp. 257–260.
15. Sack L, Holbrook NM (2006) Leaf Hydraulics. *Annual Review of Plant Biology* 57(1):361–381.

16. Rockwell FE, Michele Holbrook N, Stroock AD (2014) Leaf hydraulics I: Scaling transport properties from single cells to tissues. *Journal of Theoretical Biology* 340:251–266.
17. Buckley TN, John GP, Scoffoni C, Sack L (2017) The sites of evaporation within leaves. *Plant Physiology* 173(3):1763–1782.
18. Okano T, Bae YH, Jacobs H, Kim SW (1990) Thermally on-off switching polymers for drug permeation and release. *Journal of Controlled Release* 11(1-3):255–265.
19. Owens DE, et al. (2007) Thermally responsive swelling properties of polyacrylamide/poly(acrylic acid) interpenetrating polymer network nanoparticles. *Macromolecules* 40(20):7306–7310.
20. Flory PJ, Rehner J (1943) Statistical Mechanics of Cross-Linked Polymer Networks I. Rubberlike Elasticity. *The Journal of Chemical Physics* 11(11):512–520.
21. Flory PJ (1953) *Principles of Polymer Chemistry*. (Cornell University Press, Ithaca, NY).
22. Flory PJ, Rehner J (1943) Statistical Mechanics of Cross-Linked Polymer Networks II. Swelling. *The Journal of Chemical Physics* 11(11):521–526.
23. Tanaka T (1978) Collapse of gels and the critical endpoint. *Physical Review Letters* 40(12):820–823.
24. Janas VF, Rodriguez F, Cohen C (1980) Aging and Thermodynamics of Polyacrylamide Gels. *Macromolecules* 13(4):977–983.
25. Nicoli D, Young C, Tanaka T, Pollak A, Whitesides G (1983) Chemical modification of acrylamide gels: verification of the role of ionization in phase transitions. *Macromolecules* 16(6):887–890.
26. Dietz KJ, Herth S (2011) Plant nanotoxicology. *Trends in Plant Science* 16(11):582–589.
27. Antonietti M, Basten R, Lohmann S (1995) Polymerization in microemulsions - a new approach to ultrafine, highly functionalized polymer dispersions. *Macromolecular Chemistry and Physics* 196(2):441–466.
28. Leong YS, Candau F (1982) Inverse microemulsion polymerization. *Journal of Physical Chemistry* 86(13):2269–2271.
29. Clark HA, Hoyer M, Philbert MA, Kopelman R (1999) Optical nanosensors for chemical analysis inside single living cells. 1. Fabrication, characterization, and methods for intracellular delivery of PEBBLE sensors. *Analytical Chemistry* 71(21):4831–4836.
30. Clark HA, Kopelman R, Tjalkens R, Philbert MA (1999) Optical nanosensors for chemical analysis inside single living cells. 2. Sensors for pH and calcium and the intracellular application of PEBBLE sensors. *Analytical Chemistry* 71(21):4837–4843.
31. Munshi N, De T, Maitra a (1997) Size Modulation of Polymeric Nanoparticles under Controlled Dynamics of Microemulsion Droplets. *Journal of colloid and interface science* 190(2):387–91.
32. Nelson T, Langdale JA (1989) Patterns of leaf development in C4 plants. *The Plant cell* 1(1):3–13.
33. Langdale JA, Lane B, Freeling M, Nelson T (1989) Cell lineage analysis of maize bundle sheath and mesophyll cells. *Developmental Biology* 133(1):128–139.
34. Vincent O, Marguet B, Stroock AD (2017) Imbibition Triggered by Capillary Condensation in Nanopores. *Langmuir* 33(7):1655–1661.
35. Zhao Q, Sun J, Lin Y, Zhou Q (2010) Study of the properties of hydrolyzed polyacrylamide hydrogels with various pore structures and rapid pH-sensitivities. *Reactive and Functional Polymers* 70(9):602–609.
36. Sun H, Almdal K, Andresen TL (2011) Expanding the dynamic measurement range for polymeric nanoparticle pH sensors. *Chemical Communications* 47(18):5268–5270.
37. (2019) Fluorescein, Oregon Green and Rhodamine Green Dyes—Section 1.5, <https://www.thermofisher.com/us/en/home/references/molecular-probes-the-handbook/fluorophores-and-their-amine-reactive-derivatives/fluorescein-oregon-green-and-rhodamine-green-dyes.html>.
38. Acevedo E, Fereres E, Hsiao TC, Henderson DW (1979) Diurnal Growth Trends, Water Potential, and Osmotic Adjustment of Maize and Sorghum Leaves in the Field. *Plant Physiology* 64(3):476–480.
39. Diaspro A (2010) *Nanoscopy and Multidimensional Optical Fluorescence Microscopy*.
40. Bunt G, Wouters FS (2017) FRET from single to multiplexed signaling events. *Biophysical Reviews* 9(2):119–129.
41. Jares-Erijman EA, Jovin TM (2003) FRET imaging. *Nature Biotechnology* 21(11):1387–1395.
42. Raschke K (1970) Leaf Hydraulic System: Rapid Epidermal and Stomatal Responses to Changes in Water Supply. *Science* 167(3915):189–191.
43. Campbell GS (1986) *Soil Physics with Basic*. No. 6, pp. 367–368.
44. Brodribb TJ, Holbrook NM (2006) Declining hydraulic efficiency as transpiring leaves desiccate: Two types of response. *Plant, Cell and Environment* 29(12):2205–2215.
45. Sack L, Melcher PJ, Zwieniecki MA, Holbrook NM (2002) The hydraulic conductance of the angiosperm leaf lamina: a comparison of three measurement methods. *Journal of Experimental Botany* 53(378):2177–2184.
46. Milburn JA, Johnson RPC (1966) The conduction of sap - II. Detection of vibrations produced by sap cavitation in Ricinus xylem. *Planta* 69(1):43–52.
47. Nardini A, Salleo S (2000) Limitation of stomatal conductance by hydraulic traits: Sensing or preventing xylem cavitation? *Trees - Structure and Function* 15(1):14–24.
48. Brodribb TJ, Holbrook NM (2005) Water stress deforms tracheids peripheral to the leaf vein of a tropical conifer. *Plant Physiology* 137(3):1139–1146.
49. Blackman CJ, et al. (2014) Leaf hydraulic vulnerability to drought is linked to site water availability across a broad range of species and climates. *Annals of Botany* 114(3):435–440.
50. Rosner S, Klein A, Wimmer R, Karlsson B (2006) Extraction of features from ultrasound acoustic emissions: A tool to assess the hydraulic vulnerability of Norway spruce trunkwood? *New Phytologist* 171(1):105–116.
51. Wolkerstorfer SV, Rosner S, Hietz P (2012) An improved method and data analysis for ultrasound acoustic emissions and xylem vulnerability in conifer wood. *Physiologia Plantarum* 146(2):184–191.
52. Brodribb TJ, et al. (2016) Visual quantification of embolism reveals leaf vulnerability to hydraulic failure. *New Phytologist* 209(4):1403–1409.
53. Brodersen CR, McElrone AJ, Choat B, Matthews MA, Shackel KA (2010) The dynamics of embolism repair in xylem: In vivo visualizations using high-resolution computed tomography. *Plant Physiology* 154(3):1088–1095.
54. Holbrook NM, Ahrens ET, Burns MJ, Zwieniecki MA (2001) In vivo observation of cavitation and embolism repair using magnetic resonance imaging. *Plant Physiology* 126(1):27–31.
55. Scoffoni C, et al. (2017) Outside-xylem vulnerability, not Xylem embolism, controls leaf hydraulic decline during dehydration. *Plant Physiology* 173(2):1197–1210.
56. Trifilò P, Raimondo F, Savi T, Lo Gullo MA, Nardini A (2016) The contribution of vascular and extra-vascular water pathways to drought-induced decline of leaf hydraulic conductance. *Journal of Experimental Botany* 67(17):5029–5039.
57. Xiong D, Flexas J, Yu T, Peng S, Huang J (2017) Leaf anatomy mediates coordination of leaf hydraulic conductance and mesophyll conductance to CO₂ in Oryza. *New Phytologist* 213(2):572–583.
58. Salleo S, Raimondo F, Trifilò P, Nardini A (2003) Axial-to-radial water permeability of leaf major veins: A possible determinant of the impact of vein embolism on leaf hydraulics? *Plant, Cell and Environment* 26(10):1749–1758.
59. Cochard H, et al. (2013) Methods for measuring plant vulnerability to cavitation: A critical review. *Journal of Experimental Botany* 64(15):4779–4791.
60. Tang AC, Boyer JS (2002) Growth-induced water potentials and the growth of maize leaves. *Journal of Experimental Botany* 53(368):489–503.
61. Chunfang W, Tyree MT, Steudle E (1999) Direct measurement of xylem pressure in leaves of intact maize plants. A test of the cohesion-tension theory taking hydraulic architecture into consideration. *Plant Physiology* 121(4):1191–1205.
62. Melcher PJ, Meinzer FC, Yount DE, Goldstein G, Zimmermann U (1998) Comparative measurements of xylem pressure in transpiring and non-transpiring leaves by means of the pressure chamber and the xylem pressure probe. *Journal of Experimental Botany* 49(327):1757–1760.
63. Li Y, Sperry JS, Shao M (2009) Hydraulic conductance and vulnerability to cavitation in corn (*Zea mays L.*) hybrids of differing drought resistance. *Frontiers in Plant Science* 66(2):341–346.
64. Hammer GL, et al. (2009) Can changes in canopy and/or root system architecture explain historical maize yield trends in the U.S. corn belt? *Crop Science* 49(1):299–312.
65. Cernusak LA, et al. (2018) Unsaturation of vapour pressure inside leaves of two conifer species. *Scientific Reports* 8(1):1–7.
66. Buckley TN, Sack L (2019) The humidity inside leaves and why you should care: implications of unsaturation of leaf intercellular airspaces. *American Journal of Botany* 106(5):618–621.

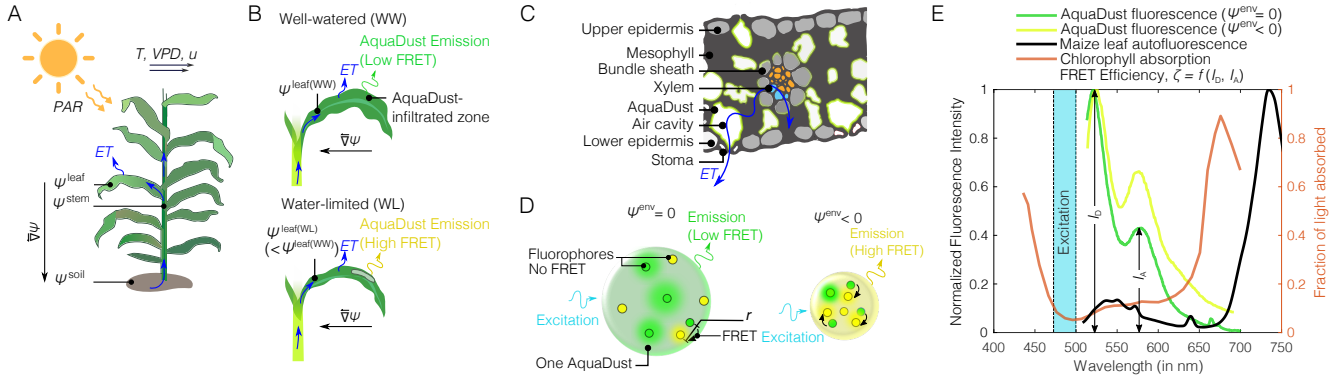


Fig. 1. AquaDust to understand water potential (ψ) driven transport in plants: (A) Schematic diagram showing AquaDust as reporter of leaf water potential (ψ^{leaf}) in intact plants in response to environmental parameters, such as photosynthetically active radiation (PAR), wind speed (u), temperature (T), and vapor pressure deficit (VPD), that regulate evapotranspiration (ET) from the leaves resulting in a negative water potential gradient ($\vec{\nabla}\psi$, $\psi^{\text{leaf}} < \psi^{\text{stem}} < \psi^{\text{soil}}$) that causes water (blue arrows) to move upwards from the soil to leaves through the stem. (B) Schematic diagrams showing leaf-scale water potential gradient ($\vec{\nabla}\psi$) develop in response to ET along the leaf lamina and our approach with AquaDust as reporter of ψ^{leaf} in a well-watered (WW) and a water-limited (WL) leaf; emission from AquaDust changes as the leaf water potential, ψ^{leaf} , gets more negative with drying of a plant. (C) Schematic diagram to show cross-section of maize leaf and localization of AquaDust with respect to mesophyll and xylem. (D) Schematic diagrams of one nanoparticle (one ‘AquaDust’): swollen, ‘wet’ state when water potential in its local environment, $\psi^{\text{env}} = 0$, (i.e. no stress condition) results in low FRET between donor (green circles) and acceptor (yellow circles) dye (left); and shrunken ‘dry’ state when $\psi^{\text{env}} < 0$ (i.e. stressed condition) results in high FRET between fluorophores, thereby, altering the emission spectra (right). (E) Fluorescent dyes are chosen to minimize reabsorption of AquaDust emission from chlorophyll; comparison of representative fluorescent emission from AquaDust (donor peak at 520 nm and acceptor peak at 580 nm) with the absorption spectra of chlorophyll and autofluorescence of maize leaf.

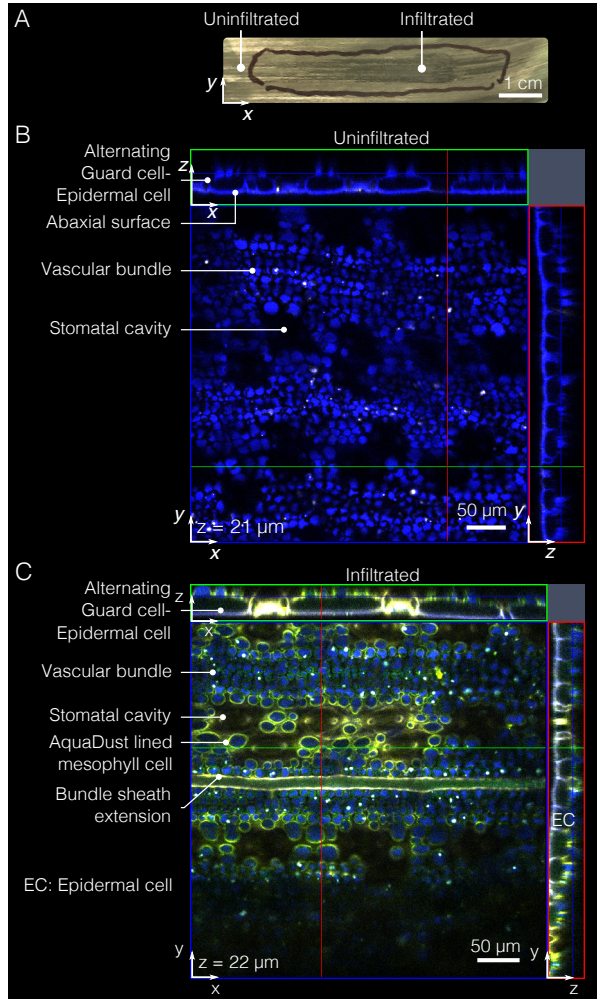


Fig. 2. Injection of AquaDust and distribution within mesophyll. (A) Typical infiltration of AquaDust suspension in maize leaf is evident with darkening of infiltrated zone immediately after infiltration; the discoloration dissipates within ~ 2 hours as the injected zone re-equilibrates with the surrounding tissue (Scale bar: 1 cm). (B) Cytosol and cuticle autofluorescence (blue) from an uninfiltrated maize leaf imaged from the abaxial side using confocal microscope with xz- and yz- planes at locations denoted by green and red lines. (C) Cytosol and cuticle autofluorescence (blue) and AquaDust fluorescence (yellow) as seen from abaxial side of maize leaf under confocal microscope infiltrated with AquaDust suspension. (See SI, Sec. S4 D for details of preparation and imaging.)

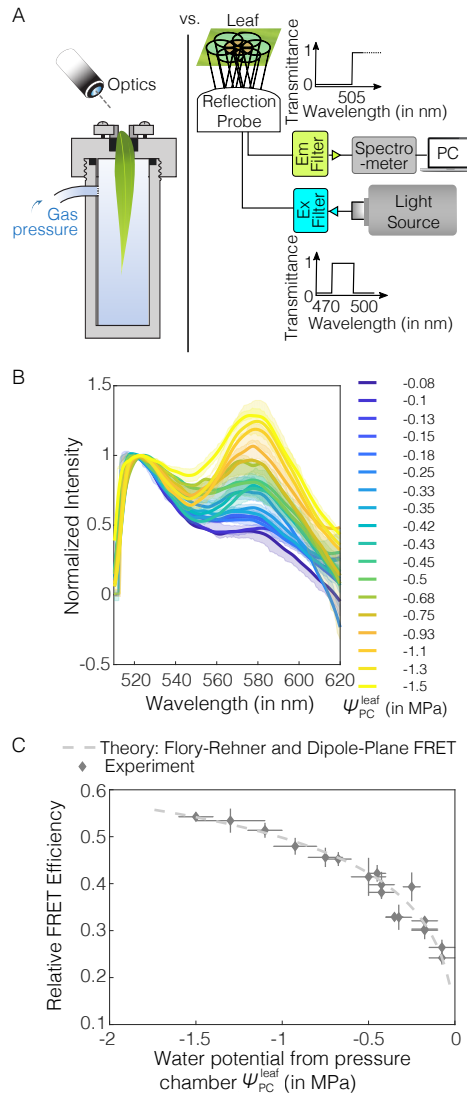


Fig. 3. AquaDust response to leaf water potential. (A) Schematic diagrams shows calibration against Scholander pressure chamber (left) and instrumentation for a typical in-situ measurement (right): A mercury lamp was used as source for illumination and a narrow-band wavelength optical filter was used to select the excitation light wavelength (here, it is 470-500 nm) used to excite AquaDust using a reflection probe. The reflected light was captured by the central fiber and sent to the spectrometer after filtering out the reflected excitation wavelengths using an emission filter to avoid the saturation of detector; spectrometer output was recorded and saved. (B) Spectra of AquaDust in maize leaves at different water potential as measured with a pressure chamber, ψ_{PC}^{leaf} on tip of actively transpiring maize leaves. Bold lines represent spectra closest to the mean FRET Efficiency and the translucent band represents the error in the spectra as obtained from 3 to 6 measurements. The legend provides mean values of ψ_{PC}^{leaf} corresponding to each spectrum. (C) Relative FRET Efficiency as calculated from the spectra in (B) is plotted against ψ_{PC}^{leaf} . A theoretical prediction as obtained from the Flory-Rehner theory and Dipole-Plane FRET model is plotted against water potential. (SI, Table S3 presents the numerical values of the plotted data.) The vertical error bars represent range of relative FRET efficiency from AquaDust and the horizontal error bars represent range of water potential from pressure chamber.

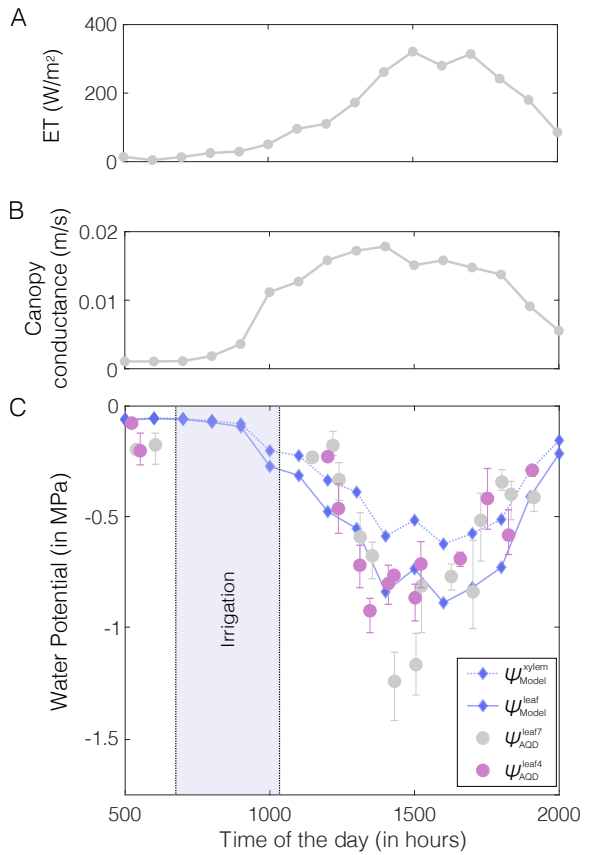


Fig. 4. In-field diurnal measurements of leaf water potential using AquaDust: (A) Calculated canopy conductance and (B) potential evapotranspiration (ET) using micrometeorological parameters such as net radiation, wind speed, temperature, and vapor pressure deficit (see SI, Fig. S14) measured in field. (C) Predicted diurnal variation of leaf water potential ($\psi_{\text{Model}}^{\text{leaf}}$) and xylem water potential ($\psi_{\text{Model}}^{\text{xylem}}$) with a soil-plant-atmosphere model driven by predicted ET from (A) (see SI, Sec. S4 N), and measured values of water potential in leaves 4 and leaves 7 with AquaDust ($\psi_{\text{AQD}}^{\text{leaf4}}$, $\psi_{\text{AQD}}^{\text{leaf7}}$). Error bars represent range of water potential from two biological replicates (plants) with three measurements per replicate.

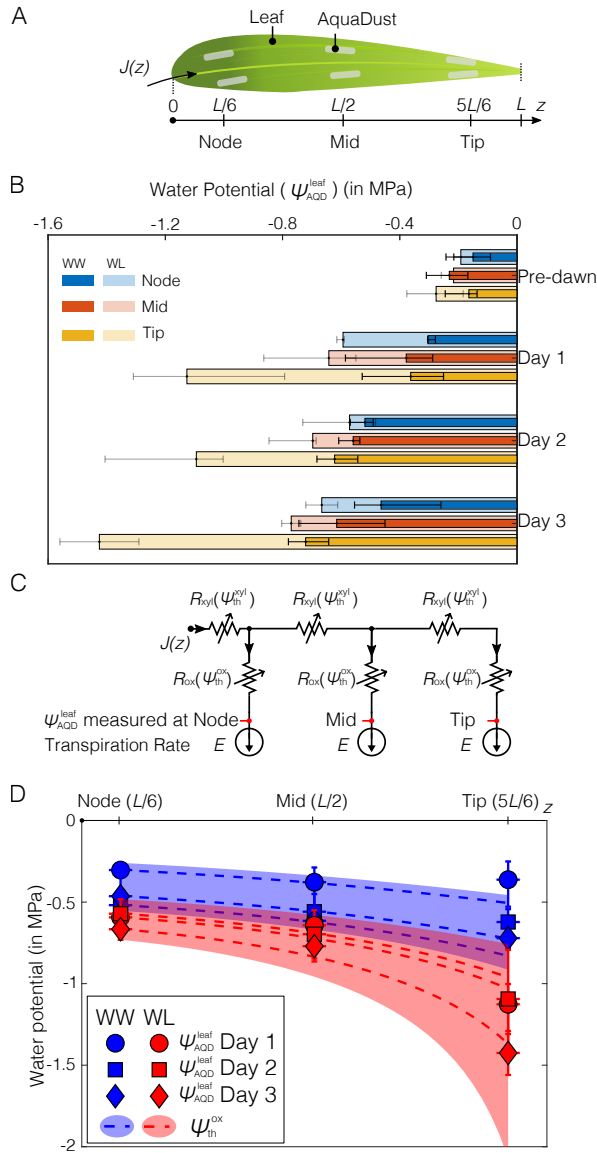


Fig. 5. Measurements of water potential gradients along a leaf: (A) Illustration of a maize leaf with AquaDust infiltrated at the node (first one-third of leaf blade connected to stem), mid (next one-third of leaf blade) and tip (final one-third of leaf blade). (B) Water potential measured using AquaDust ($\psi_{\text{AQD}}^{\text{leaf}}$) at node, mid, and tip of the leaf with maize plant in well-watered (WW) condition at pre-dawn (0500 hrs, WW Pre-dawn) and mid-day (1600 hrs) and for plants left unwatered (water-limited, WL) for 1 day (Day 1), 2 days (Day 2) and 3 days (Day 3). Bar length and error bars represent the median and the full range respectively of water potential obtained using 3 measurements per AquaDust infiltration zone on 3 different plants. (C) Comparison of $\psi_{\text{AQD}}^{\text{leaf}}$ with the prediction of mesophyll water potential ($\psi_{\text{th}}^{\text{ox}}$) using resistance-based model to predict the water potential as a function of xylem resistance (R_{xyl}) to axial flux $J(z)$ and outside-xylem resistance (R_{ox}) to transpiration flux, E where water potential from AquaDust, $\psi_{\text{AQD}}^{\text{leaf}}$ is measured at the tip, mid and node of the leaf. (D) An example of the predictions of $\psi_{\text{th}}^{\text{ox}}$ is compared against the water potential measured using AquaDust ($\psi_{\text{AQD}}^{\text{leaf}}$) from well-watered (WW) and water-limited (WL) plants. (See SI, Sec. S5 C for details of model.)